$35p$

$N65-88647$

AIAA-ASME HYPERSONIC RAMJET CONFERENCE

NAVAL ORDNANCE LABORATORY, WHITE OAK, MD. APRIL 23-25, 1963

BOUNDARY-LAYER CHANGES ACROSS
AN INCIDENT REFLECTING SHOCK

by
S. Z. PINCKNEY
NASA Langley Research Center
Langley Station, Hampton, Va.
63116

BOUNDARY-LAYER CHANGES ACROSS AN INCIDENT REFLECTING SHOCK

By S. Z. Pinckney

NASA Langley Research Center
Langley Station, Hampton, Va.

ABSTRACT

12541

A method is presented for calculating the changes in thickness and velocity profile imposed on a turbulent boundary layer by the action of an incident reflecting oblique shock. Two general methods have been utilized in previous investigations on boundary-layer-shock intersections:

(1) Momentum integral methods

(2) Assumptions of shock models and average boundary-layer parameters

The present method can be listed under method 2. The flow model used is that of a hypothetical one-dimensional boundary layer which satisfies the total momentum, mass flow, and energy of the actual boundary layer (having variable properties) upstream of the shock. Pressures in the hypothetical one-dimensional boundary layer are expressed in relation to the corresponding pressures in the free stream outside of the boundary layer. Through these expressions the static-pressure rise in the actual boundary layer is matched with that of the free stream. By use of empirical relationships arrived at from a study of experimental boundary-layer data, it has been found possible to calculate with reasonable accuracy the mass contribution from the main stream to the boundary layer as it passes through the shock.

The changes in thickness and velocity-profile index of turbulent boundary layers, as calculated by this method, are compared with experimental behavior from data of other investigators. In general the agreement between calculated and experimental results, at Mach numbers as high as 4.0 and shock turning angles to 13°, is substantially better than that obtainable with previously published methods.

BOUNDARY-LAYER CHANGES ACROSS AN INCIDENT REFLECTING SHOCK

By S. Z. Pinckney[*]

NASA Langley Research Center
Langley Station, Hampton, Va.

INTRODUCTION

A number of analytical and experimental investigations have been conducted on the behavior of boundary layers interacting with incident reflecting shock waves. The analytical treatments for the most part use one or the other of two basic lines of approach.

The first approach is that employing the momentum integral equation. Ritter and Kuo (ref. 1) used this method. The nature of their assumptions was such as to limit the applicability of their analysis to low values of Mach number and very weak shocks (on the order of 1° to 2°). Reshotko and Tucker (ref. 2) utilized the same approach as Ritter and Kuo but their method was more refined. Fair agreement with data is obtained using Reshotko and Tucker's method to calculate the changes in shape parameter and boundary-layer thickness across weak shock waves (on the order of 2° to 4°). However, the quality of the prediction deteriorates as the strength of the incident shock increases. The second method employs a hypothetical one-dimensional boundary layer having transversely constant properties that are derived from the transversely variable properties of the actual boundary layer. The overall changes occurring in the actual boundary layer are then deduced from the changes imposed on this hypothetical boundary layer in consequence of the actions occurring in a postulated boundary-layer-shock model. This approach was used by Hammitt in reference 3. Hammitt's analysis gives good results for the velocity-profile change but, as shown in figure 1, diverges from data for thickness change as the strength of the incident shock increases. Figure 1 also gives a spot value calculated using the method of Reshotko and Tucker for one of the data points of reference 4.

The present analysis, although similar in approach to that of Hammitt, employs a model for the mechanics of the hypothetical boundary-layer flow which permits evaluation of the mass contribution to the boundary layer from the external stream. Incorporation of this provision is regarded as essential to the successful estimation of the boundary-layer-thickness change.

SYMBOLS

C_M Mach number function used in the fitting of Z_2 data

H total pressure

---

[*]Aerospace Engineer.

l_1, l_2 — distances identified in figures 4 and 5

$\left(\dfrac{m}{m_l}\right)$ — mass flow per unit area ratio, $\displaystyle\int_0^1 \dfrac{\rho_b V_b}{\rho_l V_l}\, d\!\left(\dfrac{Y}{\delta}\right)$

M — Mach number

N — velocity-profile index from $\left(\dfrac{V_b}{V_l}\right) = \left(\dfrac{Y}{\delta}\right)^{1/N}$

p — static pressure

Δp — theoretical free-stream rise in static pressure across both incident and reflected shocks

q — dynamic pressure, $\dfrac{\gamma p M^2}{2}$

R_δ — Reynolds number based on δ

t — static temperature

T — total temperature

V — velocity

Y — perpendicular distance from the wall

w — mass flow in the boundary layer

Z_1 — ratio to δ_1 of the distances from the wall to the intersection of the wall shock and incident shock

Z_2 — ratio to δ_1 of the distance from the inviscid intersection of the incident shock with the wall to the most upstream point at which the pressure rise is detectable

α — turning angle through single shock wave

α_b' — angle of extra turning of the wall shock

α_b — boundary-layer-shock turning angle

β — shock angle

γ — ratio of specific heats, c_p/c_v

δ_1 — boundary-layer thickness

2

δ_d boundary-layer thickness as indicated in figures 4 and 5

ρ mass density, p/gRT

$\dfrac{\delta^*}{\delta}$ ratio of displacement thickness δ^* to boundary-layer thickness δ,

$$\int_0^1 \left(1 - \frac{\rho_b V_b}{\rho_l V_l}\right) d\left(\frac{Y}{\delta}\right)$$

$\dfrac{\delta^*}{\theta}$ shape parameter, $\dfrac{(\delta^*/\delta)}{(\theta/\delta)}$

$\dfrac{\theta}{\delta}$ ratio of momentum thickness θ to boundary-layer thickness δ,

$$\int_0^1 \frac{\rho_b V_b}{\rho_l V_l}\left(1 - \frac{V_b}{V_l}\right) d\left(\frac{Y}{\delta}\right)$$

$\dfrac{\varphi}{\varphi_l}$ momentum per unit area ratio, $\displaystyle\int_0^1 \left(\frac{\rho_b V_b{}^2}{\rho_l V_l{}^2}\right) d\left(\frac{Y}{\delta}\right)$

$\dfrac{\eta}{\eta_l}$ energy per unit area ratio, $\displaystyle\int_0^1 \left(\frac{\rho_b V_b{}^3}{\rho_l V_l{}^3}\right) d\left(\frac{Y}{\delta}\right)$

Subscripts:

b   boundary layer

d   at the point of maximum pressure rise downstream of the shock

e   effective or average

l free stream or conditions at the edge of the boundary layer

1   conditions upstream of the shock

0   stagnation conditions

'   prime values are at station δ_d'

ANALYSIS

A one-dimensional hypothetical boundary layer that has the same boundary-layer thickness, mass flow, integrated total momentum, and integrated total

enthalpy as that of the actual boundary layer is assumed. This hypothetical one-dimensional boundary layer is used, along with a boundary-layer-shock model and empirical data, to determine the changes (from a point upstream of the incident reflecting shock to the point of maximum pressure rise downstream of the shocks) in the velocity-profile index and in the boundary-layer thickness. The following assumptions were made:

(1) The flow is adiabatic.

(2) The friction effects through the region of calculation are negligible.

(3) Upstream of the shocks and at the point of maximum pressure rise downstream of the shocks, the static pressure of the actual boundary layer is constant across the boundary layer and equal to the corresponding theoretical free-stream static pressure.

(4) The velocity profiles satisfy the relation $\dfrac{V_b}{V_l} = \left(\dfrac{Y}{\delta}\right)^{1/N}$, where N is the velocity-profile index.

(5) The static-temperature profiles are of the form

$$\frac{t}{t_l} = 1 + 0.896 \frac{\gamma - 1}{2} M_l^2 \left[1 - \left(\frac{V_b}{V_l}\right)^2\right]$$

which is the form given in reference 5 for adiabatic turbulent flow.

(6) The boundary-layer-shock model assumed is of a type consistent with the boundary-layer development and shock configurations revealed by shadowgraph and schlieren observations of the actual phenomena as given in references 4, 6, 7, and 8.

(7) The expression for the integrated total enthalpy of the one-dimensional hypothetical boundary layer is as follows:

$$c_p T_e \int_0^\delta \rho_b V_b \, dY = \int_0^\delta c_p T_b \rho_b V_b \, dY$$

The necessary equations for determining the values of the equivalent boundary-layer parameters with the exception of the integrated total enthalpy are summarized in reference 9.

Profile-Index Change

Two parameters, the free-stream Mach number M_l and either the boundary-layer-profile index N or any one of the parameters of the equivalent boundary-layer flow are needed to describe completely the boundary layer except for the

absolute thickness δ. Inasmuch as $M_{l,1}$ and N_1 are known, the boundary layer upstream of the shock is completely described. The Mach number at the edge of the boundary layer downstream of the shocks $M_{l,d}$ is easily determined. To describe completely the boundary layer at the downstream station, it suffices to obtain any single equivalent flow parameter downstream of the shocks. The pressure ratio $\dfrac{p_{e,d}}{p_{l,d}}$ was chosen as the parameter to be determined. The correct value of $\dfrac{p_{e,d}}{p_{l,d}}$ must satisfy both the profile-index relationship with the free stream downstream of the incident and reflecting shocks and the boundary-layer effective static-pressure rise through the boundary-layer shocks.

Determination of $\dfrac{p_{e,d}}{p_{l,d}}$ values corresponding to the profile-index relation-
ship.- The one-dimensional hypothetical boundary-layer Mach number $M_{e,1}$ upstream of the shock can be obtained by combining the continuity, total momentum, and energy equations to obtain the effective Mach number function,

$$\frac{M_{e,1}\left(1 + \dfrac{\gamma - 1}{2}M_{e,1}^2\right)^{1/2}}{\left(1 + \gamma M_{e,1}^2\right)} = \frac{\left(\dfrac{\rho V}{\rho_0 a_0}\right)_{l,1}\left(\dfrac{t}{T}\right)_{l,1}^{1/2}\left(\dfrac{m}{m_l}\right)_1^{1/2}\left[\dfrac{N_1}{N_1 + 1} + \dfrac{\gamma - 1}{2}M_{l,1}^2\left(\dfrac{\eta}{\eta_l}\right)_1\right]^{1/2}}{\left(\dfrac{p}{H}\right)_{l,1}\left[1 + \gamma M_{l,1}^2\left(\dfrac{\varphi}{\varphi_l}\right)_1\right]} \tag{1}$$

Equation (1) is derived directly from equation (5) of reference 9 with the exception that an expression for effective total temperature based on the energy equation has been substituted for stagnation temperature, which was assumed constant across the boundary layer in reference 9. In evaluating equation (1) it will be found convenient to use plots of $\left(\dfrac{m}{m_l}\right)$, $\left(\dfrac{\varphi}{\varphi_l}\right)$, and $\left(\dfrac{\eta}{\eta_l}\right)$ presented in figures 2(a), (b), and (c) as functions of the velocity-profile index and the free-stream Mach number M_l.

Combining the continuity, momentum, and energy relationships of the equivalent boundary-layer flow and of the actual boundary-layer flow and assuming that the average energy per unit mass is the same at stations 1 and d, the following equation is obtained for the boundary layer at the downstream station:

$$\left(\frac{\gamma M_{l,d}^2}{1 + \gamma M_{e,d}^2}\right)\left(\frac{\varphi}{\varphi_l}\right)_d - \left\{\frac{M_{l,d}\left(\frac{t}{T}\right)_{l,1}^{1/2}\left[\frac{N_1}{N_1 + 1} + \frac{\gamma - 1}{2} M_{l,1}^2\left(\frac{\eta}{\eta_l}\right)_1\right]^{1/2}}{\left(\frac{t}{T}\right)_{l,d}\left(\frac{m}{m_l}\right)_1^{1/2} M_{e,d}\left(1 + \frac{\gamma - 1}{2} M_{e,d}^2\right)^{1/2}}\right\}\left(\frac{m}{m_l}\right)_d$$

$$+ \left(\frac{1}{1 + \gamma M_{e,d}^2}\right) = 0 \qquad (2)$$

For the profile-index-change calculation a simplified boundary-layer-shock model is assumed (fig. 3), which gives the same results as can be obtained for the more complicated models. By use of the shock model of figure 3, the equivalent boundary-layer flow at $M_{e,1}$ (obtained from eq. (1)) is subjected to a range of turning angles α_b to obtain a range of $M_{e,d}$ values. These $M_{e,d}$ values are substituted in equation (2) to obtain a family of equations of the form

$$a_{\alpha_b}\left(\frac{\varphi}{\varphi_l}\right)_d - b_{\alpha_b}\left(\frac{m}{m_l}\right)_d + c_{\alpha_b} = 0 \qquad (3)$$

where for a given value of α_b, a, b, and c are constants. The solution of equation (3) for each selected value of α_b is a function of the velocity-profile index N_d and of the free-stream Mach number $M_{l,d}$. The Mach number $M_{l,d}$ is determined from the external stream conditions. Thus, the solution of each equation (3) for N_d can be obtained by using figures 2(a) and (b). With the values of $M_{l,d}$ and N_d known, the corresponding $p_{e,d}/p_{l,d}$ values can be evaluated from the equation

$$\frac{p_{e,d}}{p_{l,d}} = b_{\alpha_b}\left(\frac{m}{m_l}\right)_d \qquad (4)$$

The values of $\left(m/m_l\right)_d$ are determined for the N_d value obtained by solutions of equation (3). Having obtained solutions for N_d and $p_{e,d}/p_{l,d}$ as a function of α_b through the conservation equations relating the equivalent flow and the actual boundary-layer flow at station d, the next step is to obtain a second set of solutions for $p_{e,d}/p_{l,d}$ through values obtained from the effective boundary-layer-shock system.

Determination of $p_{e,d}/p_{l,d}$ values corresponding to the effective static-pressure ratio through the boundary-layer shocks.- Corresponding to the range of

$M_{e,d}$ values obtained in the previous section by subjecting $M_{e,1}$ to a range of turning angles by using the shock model of figure 3, a range of effective static-pressure ratios $p_{e,d}/p_{e,1}$ is obtained. This range of $p_{e,d}/p_{e,1}$ values is then used to obtain $p_{e,d}/p_{l,d}$ as a function of α_b from the following equation:

$$\frac{p_{e,d}}{p_{l,d}} = \left[\frac{1 + \gamma M_{l,1}^2 \left(\frac{\varphi}{\varphi_l}\right)_1}{1 + \gamma M_{e,1}^2} \right] \frac{\left(\frac{p_{e,d}}{p_{e,1}}\right)}{\left(\frac{p_{l,d}}{p_{l,1}}\right)} \tag{5}$$

The pressure ratio $p_{l,d}/p_{l,1}$ is the theoretical static-pressure ratio across both incident and reflected shocks in the free stream.

Graphical solution for $p_{e,d}/p_{l,d}$.- Superposition of the two sets of values of $p_{e,d}/p_{l,d}$ as functions of α_b obtained as described in the preceding sections yields a graphical solution for the unique value of $p_{e,d}/p_{l,d}$ which satisfies simultaneously the requirements of the boundary layer and of the external stream and thereby determines the correct value of the boundary-layer-shock turning angle α_b. The value of N_d is then immediately determinate from the value of α_b.

Boundary-Layer-Thickness Change

The boundary-layer-thickness change across the shock system is calculated from the equations of continuity applied in a direction parallel to the wall. It is essential that provision be made for the effects of mass transferred from the external stream to the boundary layer in passing through the shock system and the following mixing region up to the point of maximum pressure rise. The very simple boundary-layer-shock model successfully used in the previous section to calculate the profile-index change permits no mass-flow addition to the boundary layer and is unsuitable for thickness-change calculations. It becomes necessary therefore to introduce a somewhat more elaborate model which recognizes the effects of mass addition.

The models selected, illustrated in figures 4 and 5, incorporate a shock originating at the wall representative of the effect of the thickening which occurs in the inner part of the actual boundary layer under the influence of an adverse pressure gradient. A procedure has been evolved for arriving at the strength and point of origin of this wall shock such that the mass flow in the boundary layer can be deduced from the distance from the wall of the boundary-layer outer streamline. The turning of the equivalent boundary layer by this wall shock creates a void region in the flow model contiguous to the wall. Some further elaboration of the flow model incorporates features suggested by study

of schlieren pictures of the terminal development of the boundary-layer flow to the point of maximum pressure rise.

Mass addition to the boundary layer through the shocks.- The point of origin (fig. 4 or 5) of the wall shock is determined by knowing the shock turning angle and the distance from the wall $\left(Z_1 \delta_1\right)$ to the point of intersection with the incident shock. The value of Z_1 (ratio to δ_1 of the distance from the wall to the intersection of the wall shock and incident shock) is obtained from functional relationships empirical in origin. With the point of origin of the wall shock and the turning angle known, the fore part of the void region can be described. After the incident shock intersects with the wall shock it passes on to intersect with the void region. The wall shock passes from the point of origin out until it intersects the boundary-layer edge. The height of the void region is then calculated at the longitudinal location of the intersection of the incident shock with the void region or at the longitudinal location of the intersection of the wall shock with the boundary-layer edge, whichever point is farther downstream. The boundary-layer thickness at this position is referred to as δ_d'. Study of the boundary-layer mass flows in comparison with values calculated from the preceding flow model, with various assumptions being used for the strength of the wall shock, revealed an interesting proportionality. At turning angles of α_b within the equivalent boundary layer, for both the incident shock and the wall shock, the boundary-layer flow calculated for a thickness δ_d' (at values of $\rho_e V_e$ corresponding to the state of the equivalent boundary layer at this station) generally was about 8 to 12 percent less than the measured boundary-layer mass flow at the point of maximum pressure rise. Thus, the height of the void region at the station designated by thickness δ_d' was nearly a measure of the exact mass addition to the boundary layer.

The postulated strength of the wall shock was increased slightly by stipulating a turning angle greater than the angle α_b by a small angle α_b'. This change served to establish equality between the measured boundary-layer-flow addition and that calculated, as indicated, from the height of the void region. The requisite values of α_b' were determined for the available data and are presented in figure 6 plotted against the free-stream turning angle of the incident shock. Within the range of the data investigated, no systematic trend with Reynolds number, Mach number, or incident shock strength was evident. The assumption, in the light of this result, that α_b' can be given a fixed value of 2°, for the range of conditions explored, forms the basis of the method given here for calculating the mass addition to the boundary layer and, from this result, the change in thickness. It remains now to outline the process of making the calculation.

Outline of calculations.- The calculated mass-flow ratio across the shocks is given by

$$\frac{w_d'}{w_1} = \left(\frac{p_{e,d}'}{p_{e,1}}\right)\left(\frac{M_{e,d}'}{M_{e,1}}\right)\left[\frac{1 + \frac{\gamma-1}{2}\left(M_{e,d}'\right)^2}{1 + \frac{\gamma-1}{2}M_{e,1}^2}\right]\left(\frac{\delta_d'}{\delta_1}\right) \tag{6}$$

The equivalent flow parameters $M_{e,d}'$ and $p_{e,d}'$ are obtained by subjecting the equivalent flow at station 1 to a total turning of $\left(2\alpha_b + 2^o\right)$. In order to calculate δ_d'/δ_1 the value of Z_1 is needed, as is the turning angle and the shock angle of each of the shock waves of the boundary-layer-shock models (figs. 4 and 5). An empirical correlation has been established for Z_1, which is illustrated in figure 7. The value of Z_1 for a given set of conditions is a function of shock turning angle, Mach number, and Reynolds number. Details of the correlation are given in the appendix. The various shock angles and lengths required to determine the mass-flow addition through evaluation of δ_d'/δ_1 can be computed using conventional two-dimensional, oblique shock characteristic methods. The necessary equations are summarized in the appendix.

The continuity equation written between stations 1 and d with the inclusion of the calculated mass-flow ratio across the shocks gives for the overall boundary-layer-thickness ratio δ_d/δ_1.

$$\frac{\delta_d}{\delta_1} = \frac{w_d'}{w_1} \frac{\rho_{l,1} V_{l,1}\left(\frac{m}{m_l}\right)_1}{\rho_{l,d} V_{l,d}\left(\frac{m}{m_l}\right)_d} \tag{7}$$

where w_d'/w_1 is calculated by assuming the wall-shock turning to be $\left(\alpha_b + 2^o\right)$.

RESULTS AND DISCUSSION

Profile-Index Change

The method given for calculating a change in profile index N was derived with the assumption that the boundary-layer-velocity distribution was truly exponential. A value of N, for purposes of analysis, may be associated with an actual boundary-layer-velocity profile, not truly exponential. This purpose is accomplished by stipulating that the value of N to be assumed for the actual profile corresponds to a truly exponential profile having a value of $\left(\varphi/\varphi_l\right)$ identical with that of the actual boundary layer. The quality of the results obtained by using the exponential assumption is evidenced by figure 8, which shows data points and curves calculated by the procedure outlined in a previous section. The greatest deviation found in the cases analyzed was of the order of 10 percent.

Boundary-Layer-Thickness Change

Curves of δ_d/δ_1 as a function of α_l, calculated by methods outlined herein, are shown in figure 9 at values corresponding to the data of references 4, 6, and 7. Only data from experiments for which the shock generator completely spanned the tunnel have been used. Figure 9 shows the experimental value of δ_d/δ_1 for $\alpha_l = 4^\circ$ obtained from reference 4 about 10 percent above the calculated δ_d/δ_1 value. A study of the parameters used in the calculation of δ_d/δ_1 showed that the calculated value of Z_2 (and thus the value of Z_1) was approximately 10 percent lower than the experimental value. Recalculation of the δ_d/δ_1 curve, using the experimental values of Z_2 instead of the calculated values, brought the calculated δ_d/δ_1 values to within 3 percent of the experimental values. The difference between the experimental and calculated Z_2 values is perhaps a consequence of three-dimensional effects. Except for the previously discussed discrepancy, the calculated boundary-layer-thickness change agrees within 5 percent of the experimental values.

As the present empirical curves used in the calculation of δ_d/δ_1 are based largely on the data of references 4, 6, and 7 it is not surprising that the calculated curves of δ_d/δ_1 correspond reasonably well with the experimental curves. Demonstration of the general applicability of this empirical procedure for calculating the development of turbulent boundary layers under impinging reflecting shocks, both within the range explored and by extension to broader ranges of Reynolds number, Mach number, and shock strength, awaits the acquisition of new data.

CONCLUDING REMARKS

In the light of the present investigation of the interaction between an incident-reflecting oblique shock system and a two-dimensional, supersonic, turbulent boundary layer the following statements can be made relative to the changes in the boundary layer between a point upstream where the interaction starts and the downstream point where the maximum pressure rise occurs:

1. With regard to the analytical procedure for calculating the change in the profile index:

    (a) The profile-index-change calculation requires no empirical information or knowledge of the boundary-layer-thickness change.

    (b) Values of N change calculated at Mach number 3.0 and turning angle up to 11° are found to agree with data to within 10 percent or better.

2. With regard to the empirical procedure for correlating data of boundary-layer-thickness change:

10

(a) The boundary-layer-shock model assumed is of a type consistent-with the boundary-layer development and shock configuration revealed by shadowgraph and schlieren observations of the actual phenomena.

(b) Data in the Mach number range 2.9 to 3.85, Reynolds number range $\left(R_\delta\right)$ of 1.7×10^5 to 5.82×10^5, and for turning angles through the free-stream incident shock up to 13° are correlated to within 5 percent.

(c) The next steps will be preparation of a format designed for ready utility and, as data become available, exploration of the range of applicability.

EMPIRICAL CORRELATION OF Z_1 AND DETERMINATION OF $\delta_d^{'}/\delta_1$

At present the value of Z_1 is most easily obtained from the empirical curve of Z_1/Z_2 as a function of $\Delta p/q_{l,1}$ in figure 10 and the empirical relation for Z_2 (ratio to δ_1 of the distance from the inviscid intersection of the incident shock with the wall to the most upstream point at which the pressure rise is detectable),

$$Z_2 = C_{M_{l,1}}\left(R_\delta^{0.0685M_{l,1}}\frac{\Delta p}{q_{l,1}}\right)^d \tag{8}$$

The exponent d is given by the expression

$$d = 1.406e^{-0.0202M_{l,1}}\left[0.48e^{-8.83\left(M_{l,1}-2.9\right)^2} + 1\right]$$

The empirically determined Mach number function $C_{M_{l,1}}$ is given in figure 11.

The quality of correlation of Z_2 (calculated) versus Z_2 (from the experimental data) can be seen in figure 12. The range of the data and the types of data (wedge or reflected shock) used in figure 12 are presented in table I. These data are from references 4, 6, 7, 8, and 10 to 14.

The shock-wave angles and the corresponding turning angles of the boundary-layer-shock models (figs. 4 and 5) are presented in the following table:

Shock angle	Turning angle
$\beta_{b,1}$	α_b
$\beta_{b,1}^{'}$	$\alpha_b + 2^{\circ}$
$\beta_{b,2}$	$\alpha_b + 2^{\circ}$
$\beta_{b,2}^{'}$	α_b
$\beta_{l,1}^{'}$	$\alpha_l + 2^{\circ}$
$\beta_{l,2}$	α_l

The evaluation of δ_d'/δ_1, obtained from the values of the shock-wave angles and the corresponding turning angles of the boundary-layer-shock models along with the calculated value of Z_1, depends on which of three cases is applicable. The three cases and the corresponding equation of δ_d'/δ_1 for each are:

Case 1: For $l_2 \geqq l_1$ and $(Z_1\delta_1) < \delta_1$ (where l_1 and l_2 are indicated in fig. 4(b)), l_2/δ_1 is given by

$$\frac{l_2}{\delta_1} = \frac{Z_1}{\tan \beta_{b,1}'} + \left\{\left[\frac{\sin(\beta_{b,1} - \alpha_b)\sin(\beta_{b,2} - \alpha_b)}{\sin \beta_{b,1} \sin \beta_{b,2} \tan(\beta_{b,2} - \alpha_b)}\right](1 - Z_1)\right\} \qquad (9)$$

and l_1/δ_1 is given by

$$\left(\frac{l_1}{\delta_1}\right) = Z_1\left\{\frac{1}{\tan \beta_{b,1}'} + \frac{1}{\tan\left[\beta_{b,2}' - (\alpha_b + 2^\circ)\right]}\right\}\frac{\sin\left[\beta_{b,2}' - (\alpha_b + 2^\circ)\right]\cos(\alpha_b + 2^\circ)}{\sin \beta_{b,2}'} \qquad (10)$$

When l_2, l_1, and $(Z_1\delta_1)$ satisfy the conditions of Case 1 the following expression for δ_d'/δ_1 is used:

$$\left(\frac{\delta_d'}{\delta_1}\right) = \left\{\left[\frac{\sin(\beta_{b,1} - \alpha_b)\sin(\beta_{b,2} - \alpha_b)}{\sin \beta_{b,1} \sin \beta_{b,2}}\right](1 - Z_1)\right\} + Z_1 \qquad (11)$$

Case 2: For $l_2 < l_1$ and $(Z_1\delta_1) \leqq \delta_1$ (fig. 4), equations (9) and (10) are used for l_2/δ_1 and l_1/δ_1. When l_2, l_1, and $(Z_1\delta_1)$ satisfy the conditions of Case 2, the following equation for δ_d'/δ_1 is used:

$$\left(\frac{\delta_d'}{\delta_1}\right) = \left\{\left[\frac{\sin(\beta_{b,1} - \alpha_b)\sin(\beta_{b,2} - \alpha_b)}{\sin \beta_{b,1} \sin \beta_{b,2}}\right](1 - Z_1)\right\} + Z_1 + \frac{l_1 - l_2}{\delta_1}\tan 2^\circ \qquad (12)$$

Case 3: For $l_2 < l_1$ and $(Z_1\delta_1) > \delta_1$ (l_2 and l_1 are indicated in fig. 5(b)), the following equation for δ_d'/δ_1 is used:

$$\frac{\delta_d'}{\delta_1} = \left\{ \left[\frac{\sin\left(\beta_{l,1}' - \alpha_b\right)\sin\left(\beta_{l,2} - \alpha_l\right)}{\sin\beta_{l,1}' \, \sin\beta_{l,2}} \right] \left(1 - Z_1\right) \right\} + Z_1 + \frac{l_1 - l_2}{\delta_1} \tan 2^\circ \qquad (13)$$

with l_2/δ_1 given by

$$\frac{l_2}{\delta_1} = \frac{\left\{ \left[\dfrac{\sin\left(\beta_{l,1}' - \alpha_b\right)\sin\left(\beta_{l,2} - \alpha_l\right)}{\sin\beta_{l,1}' \, \sin\beta_{l,2}} \right]\left(1 - Z_1\right) \right\} + Z_1 - 1}{\tan\left(\alpha_b + 2^\circ\right)} + \frac{1}{\tan\beta_{b,1}'} \qquad (14)$$

and l_1/δ_1 given by

$$\frac{l_1}{\delta_1} = \frac{\sin\left[\beta_{b,2}' - \left(\alpha_b + 2^\circ\right)\right]\cos\left(\alpha_b + 2^\circ\right)}{\sin\beta_{b,2}'} \left\{ \frac{l_2}{\delta_1} + \frac{\left[\dfrac{\sin\left(\beta_{l,1}' - \alpha_b\right)\sin\left(\beta_{l,2} - \alpha_l\right)}{\sin\beta_{l,1}' \, \sin\beta_{l,2}} \right]\left(1 - Z_1\right) + Z_1}{\tan\left[\beta_{b,2}' - \left(\alpha_b + 2^\circ\right)\right]} \right\} \qquad (15)$$

14

REFERENCES

1. Ritter, Alfred, and Kuo, Yung-Huai: Reflection of a Shock Wave From a Bound-
   ary Layer Along a Flat Plate. I - Interaction of Weak Shock Waves With Lam-
   inar and Turbulent Boundary Layers Analyzed by Momentum-Integral Method.
   NACA TN 2868, 1953.

2. Reshotko, Eli, and Tucker, Maurice: Effect of a Discontinuity on Turbulent
   Boundary-Layer-Thickness Parameters With Application to Shock-Induced Sep-
   aration. NACA TN 3454, 1953.

3. Hammitt, Andrew G.: The Interaction of Shock Waves and Turbulent Boundary
   Layers. Jour. Aero. Sci., June 1958, p. 345.

4. Kepler, C. E., and O'Brien, R. L.: Supersonic Turbulent Boundary Layer
   Growth over Cooled Walls in Adverse Pressure Gradients. United Aircraft
   Report, ASD-TDR-62-87, Oct. 1962.

5. Persh, Jerome, and Lee, Roland E.: Tabulation of Compressible Turbulent
   Boundary Layer Parameters. NAVORD Rep. 4282 (Aeroballistic Res. Rep. 337),
   U.S. Naval Ord. Lab. (White Oak, Md.), May 1, 1956.

6. Kepler, C. E., and Sanlorenzo, E.: A Study of Shock Wave Turbulent Boundary
   Layer Interaction at M = 3.0. Princeton Univ. Rept. No. 222, July 1953.

7. Vas, I. E., and Bogdonoff, S. M.: Interaction of a Shock Wave With a Turbul-
   ent Boundary Layer at M = 3.85. Princeton Univ. Rept. No. 294,
   Apr. 11, 1955.

8. Bardsley, O., and Mair, W. A.: The Interaction Between an Oblique Shock-
   Wave and a Turbulent Boundary Layer. Phil. Mag., ser. 7, vol. 42, no. 324,
   Jan. 1951, pp. 29-36.

9. Wyatt, DeMarquis D.: Analysis of Errors Introduced by Several Methods of
   Weighting Nonuniform Duct Flows. NACA TN 3400, 1955.

10. Liepmann, H. W., Roshko, A., and Dhawan, S.: On Reflection of Shock Waves
    From Boundary Layers. NACA Rep. 1100, 1952. (Supersedes NACA TN 2334.)

11. Kuehn, Donald M.: Experimental Investigation of the Pressure Rise Required
    for the Incipient Separation of Turbulent Boundary Layers in Two-Dimensional
    Supersonic Flow. NASA MEMO 1-21-59A, 1959.

12. Chuan, Raymond L.: An Investigation of Shock-Wave Boundary Layer Interaction.
    Univ. of Southern Calif. Rept. No. 40-201, Aug. 1955.

13. Sterrett, James R., and Emery, James C.: Experimental Separation Studies for
    Two-Dimensional Wedges and Curved Surfaces at Mach Numbers of 4.8 to 6.2.
    NASA TN D-1014, 1962.

14. Hammitt, A. G., Vas, I. E., and Hight, S.: An Analysis of the Effect of
     Shock Waves on Turbulent Boundary Layers. Princeton Univ. Rept. No. 396,
     July 1957.

TABLE I

RANGE OF VARIABLES USED IN EMPIRICAL CORRELATIONS

Reference	Mach number range	Wall static distribution	α_l range	Type of data	Shadowgraph or schlieren pictures	Reynolds number range, R_δ	Boundary-layer surveys
7	≈ 3.85	Yes	4° through 13°	Reflected shock	Yes	$\approx 5.82 \times 10^5$	No
6	≈ 2.97	Yes	7° through 15°	Reflected shock	Yes	$\approx 2.70 \times 10^5$	For $\alpha_l = 10°$
10	≈ 1.44	Yes	3° through 4.5°	Reflected shock	For $\alpha_\infty = 4.5°$ No	$\approx 1.42 \times 10^4$	Upstream
11	≈ 2.99 to 3.09	Yes	4.6° through 11.6°	Reflected shock	No	≈ 4.8 to 5.1×10^4	No
11	≈ 2.33 to 4.01	Yes	25° and 30°	Wedge shock	Yes	≈ 3.5 to 4.4×10^4	No
12	≈ 2.54	Yes	22.9°	Wedge shock	Yes	$\approx 4.0 \times 10^3$	No
13	≈ 5.8 to 6.2	Yes	15° through 34°	Wedge shock	At 8° and 28° for M = 5.8	≈ 2.3 and 2.76×10^6	Upstream
14	≈ 2.97	Yes	7° through 11°	Reflected shock	No	$\approx 1.81 \times 10^5$	Yes
4	≈ 3.0	Yes	4° through 10°	Reflected shock	For 8° but not clear	$\approx 1.70 \times 10^5$	Yes
8	≈ 1.965	No	2.9° through 15.2°	Reflected shock	Yes	$\approx 5.36 \times 10^4$	Upstream

NASA

HAMMITT, REF. 3
RESHOTKO & TUCKER, $M_l = 3.0$, REF. 2

REF. DATA M_l
7 —— ○ —— 3.85
6 —— □ —— 2.97
4 —— ◇ —— 3.00

WEAK SHOCK
$M_l = 3$
$M_l = 4$

STRONG SHOCK
$M_l = 3$
$M_l = 4$

$\left(\dfrac{\delta_d}{\delta_1}\right)$

1.4
1.2
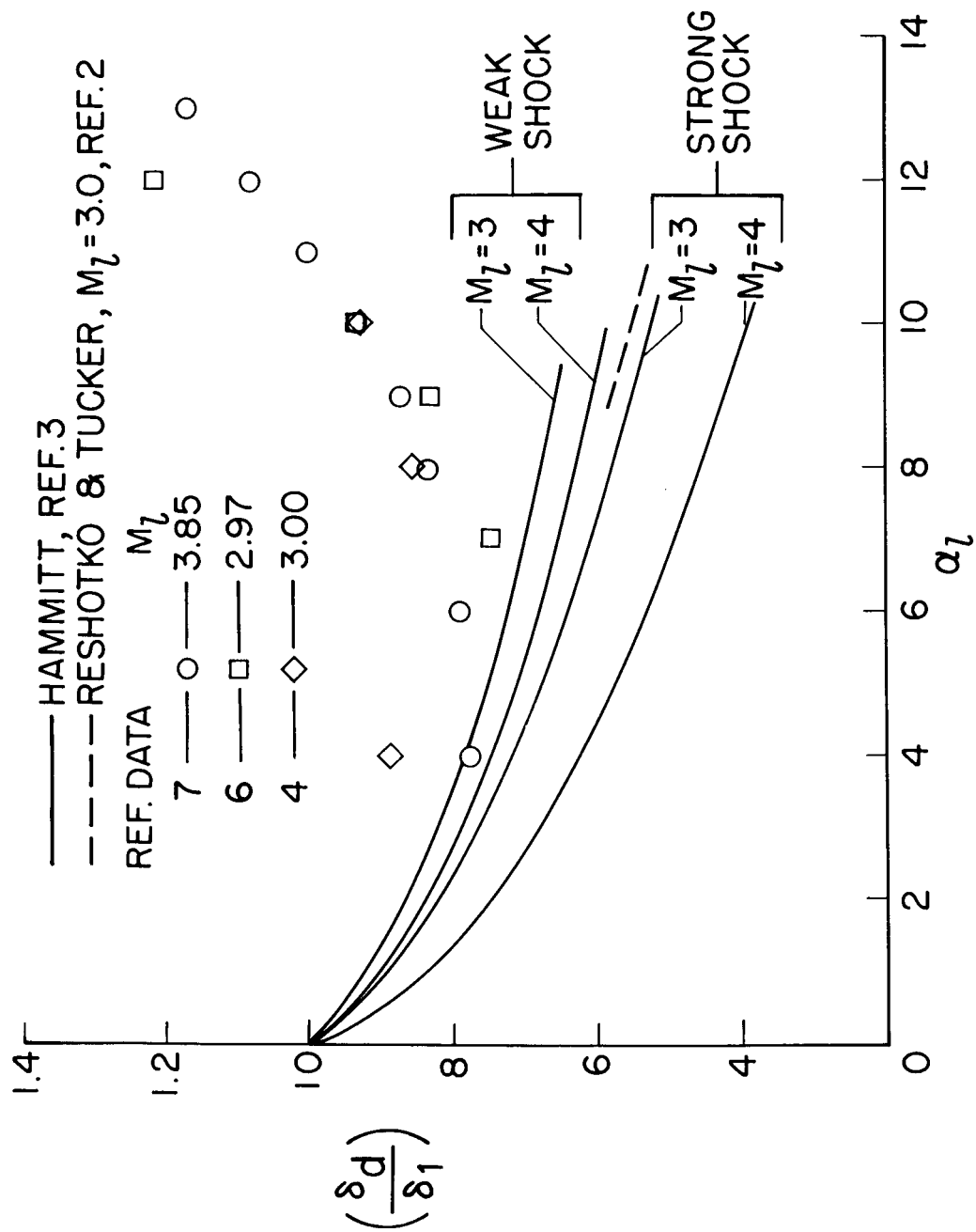1.0
.8
.6
.4

0   2   4   6   8   10   12   14

α_l

Figure 1.- $\dfrac{\delta_d}{\delta_1}$ ratio versus free-stream turning angle α_l.
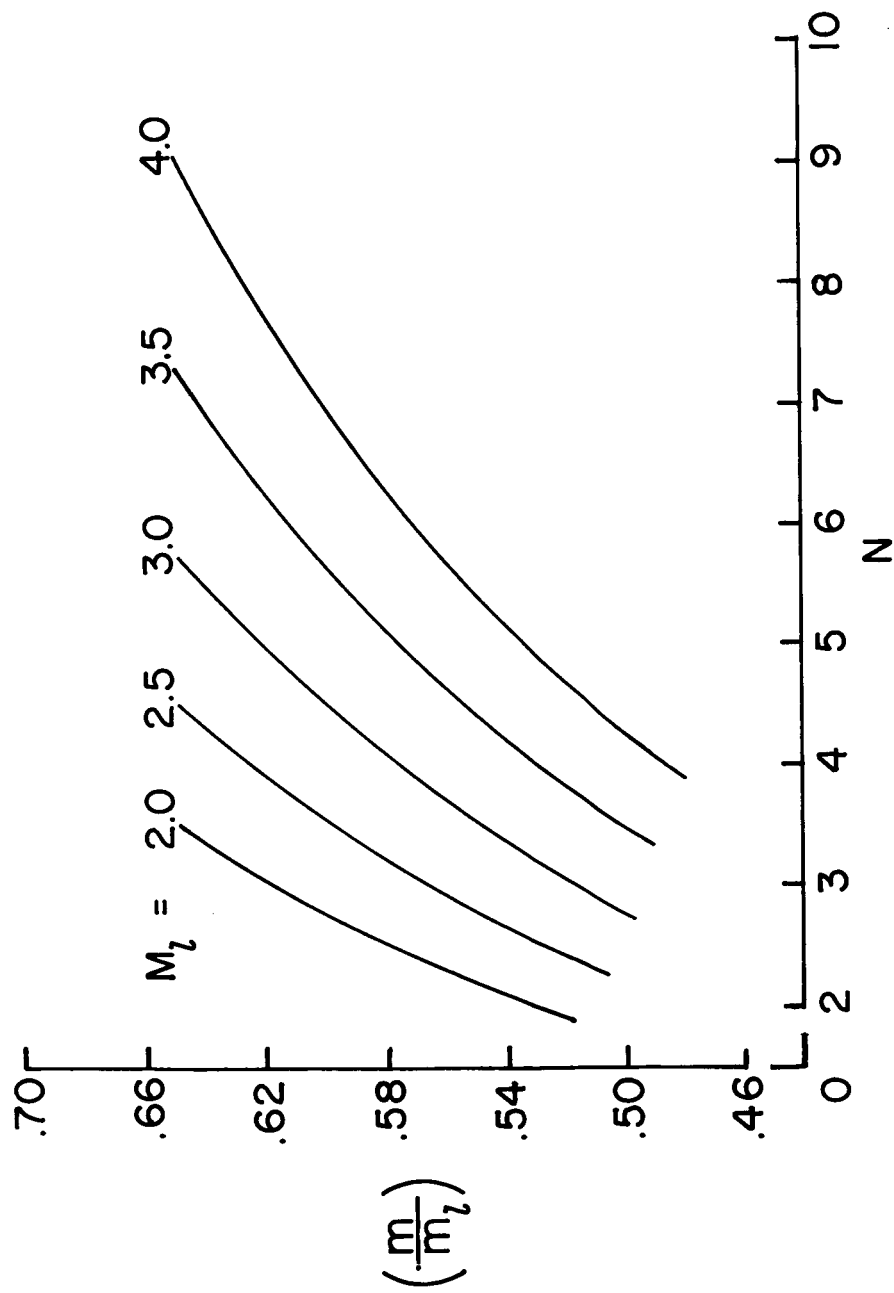
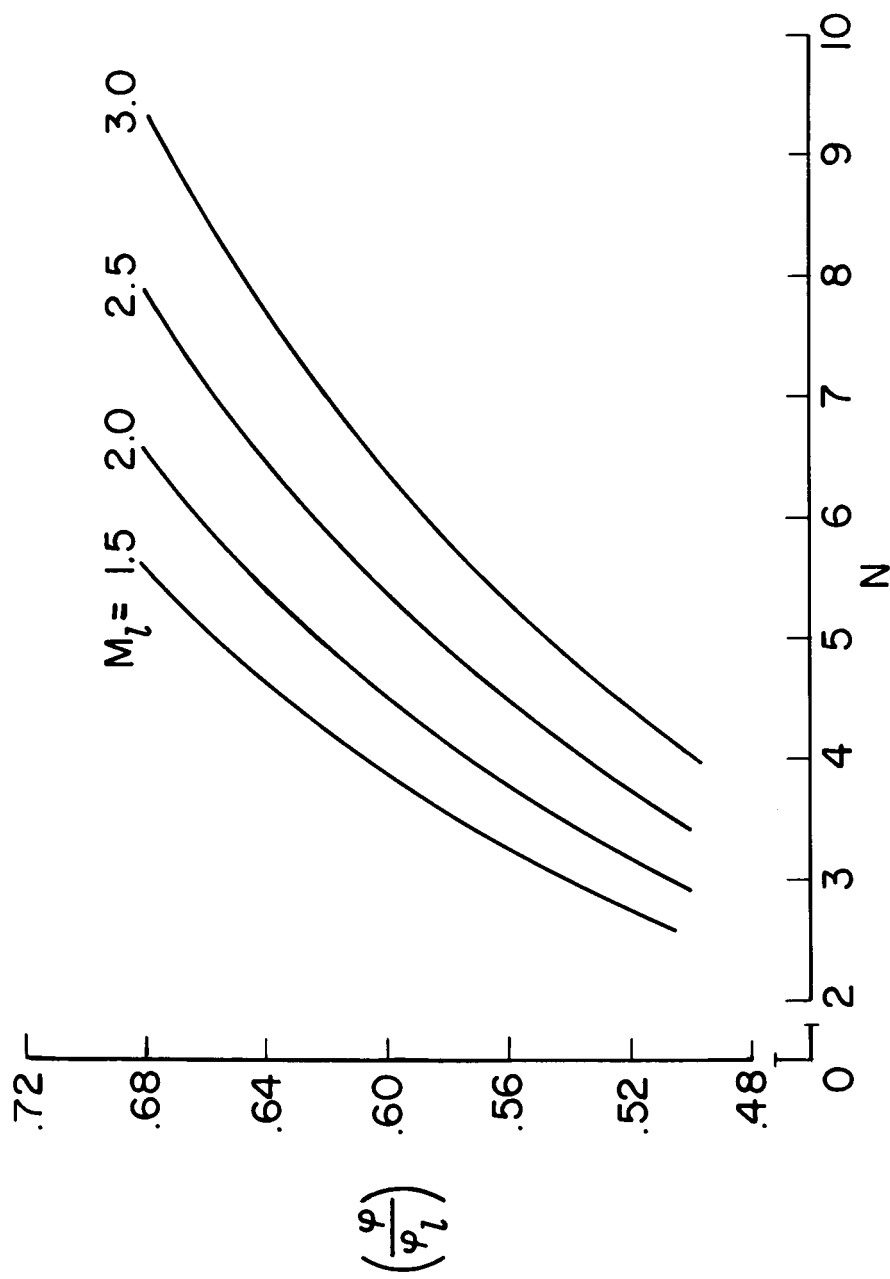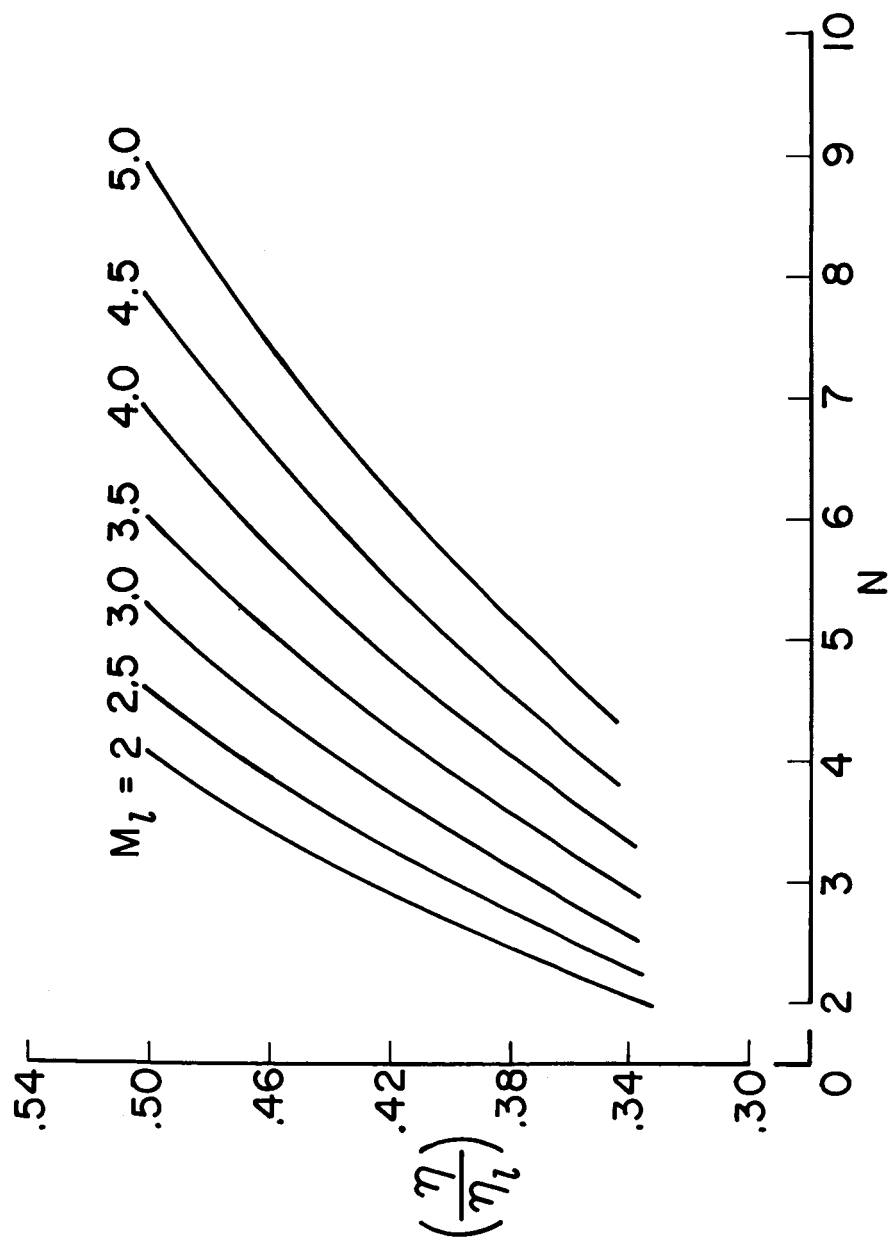Figure 2(a).- Plot of $\left(\dfrac{m}{m_l}\right)$ versus N for constant M_l.

NASA

Figure 2(b).- Plot of $\left(\dfrac{\varphi}{\varphi_l}\right)$ versus N for constant M_l.

NASA

Figure 2(c).- Plot of $\left(\dfrac{\eta}{\eta_l}\right)$ versus N for constant M_l.

NASA

NASA
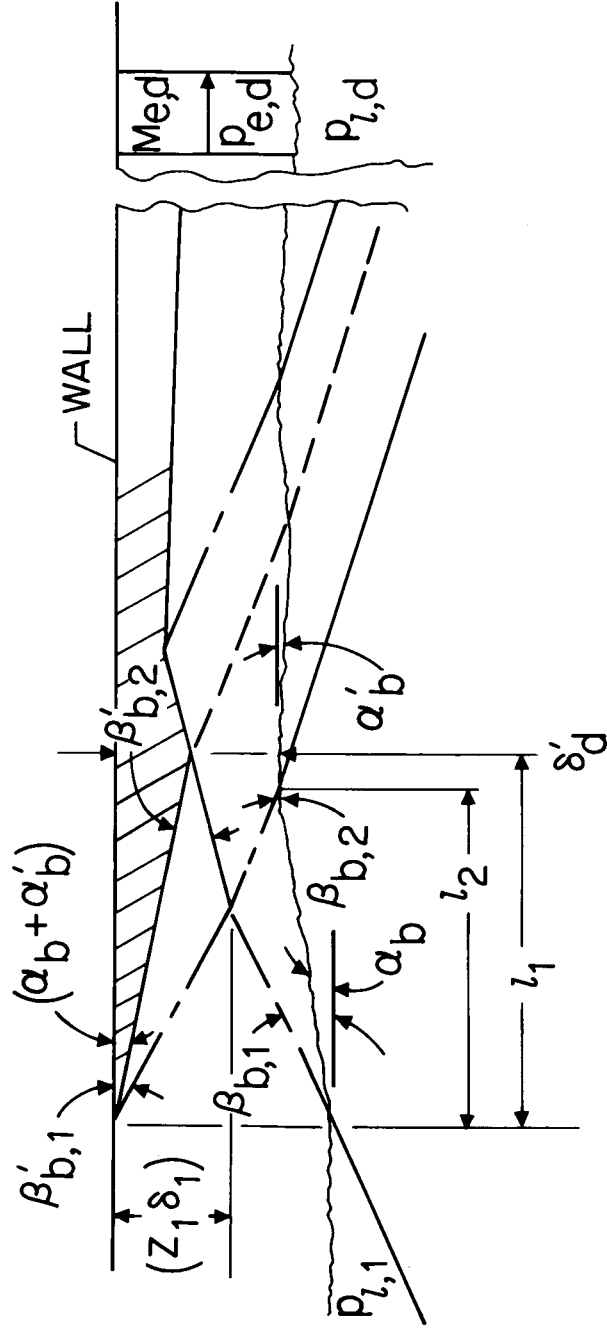
B.L. SHOCK (2)
WITH TURNING = α_b

$M_{e,d}$

$p_{e,d}$

$M_{l,d}$, $p_{l,d}$

FREE STREAM
REFLECTED SHOCK
TURNING = α_l

FREE STREAM
INCIDENT SHOCK
TURNING = α_l

B.L. SHOCK (1)
WITH TURNING = α_b

$M_{e,1}$

$p_{e,1}$

$M_{l,1}$, $p_{l,1}$
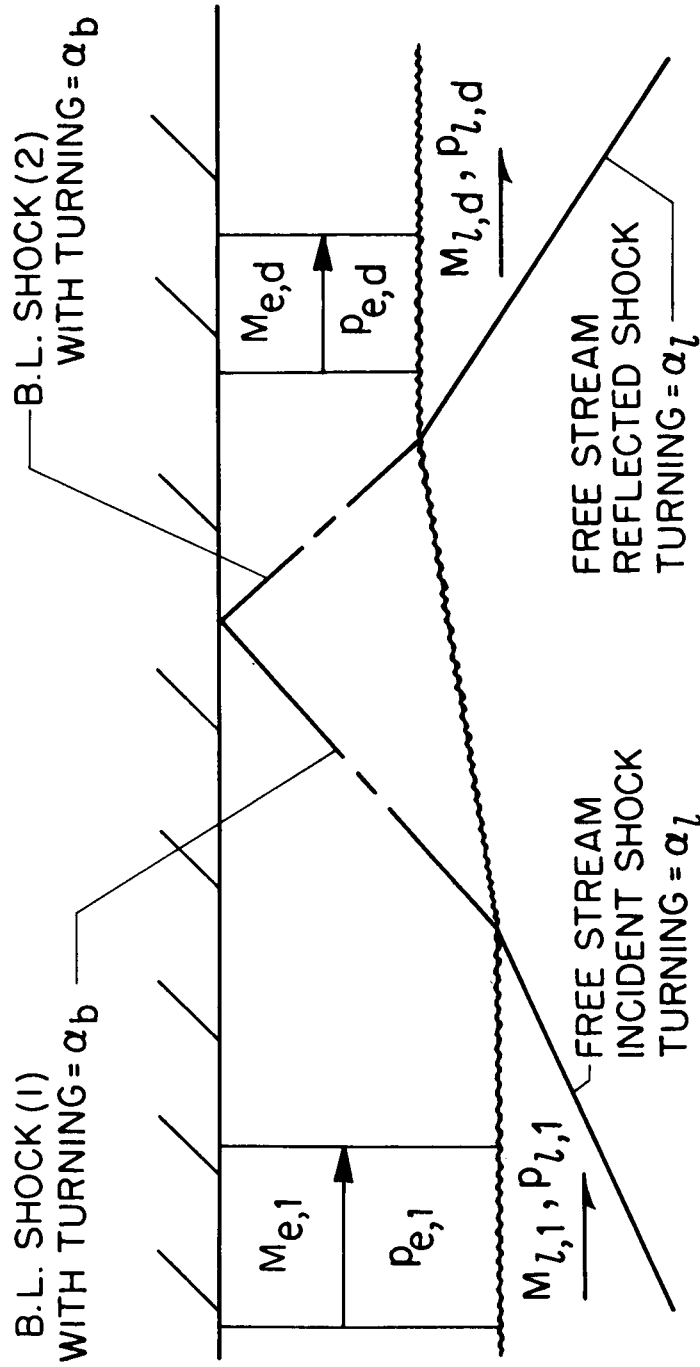
Figure 3.- Simplified boundary-layer shock model.
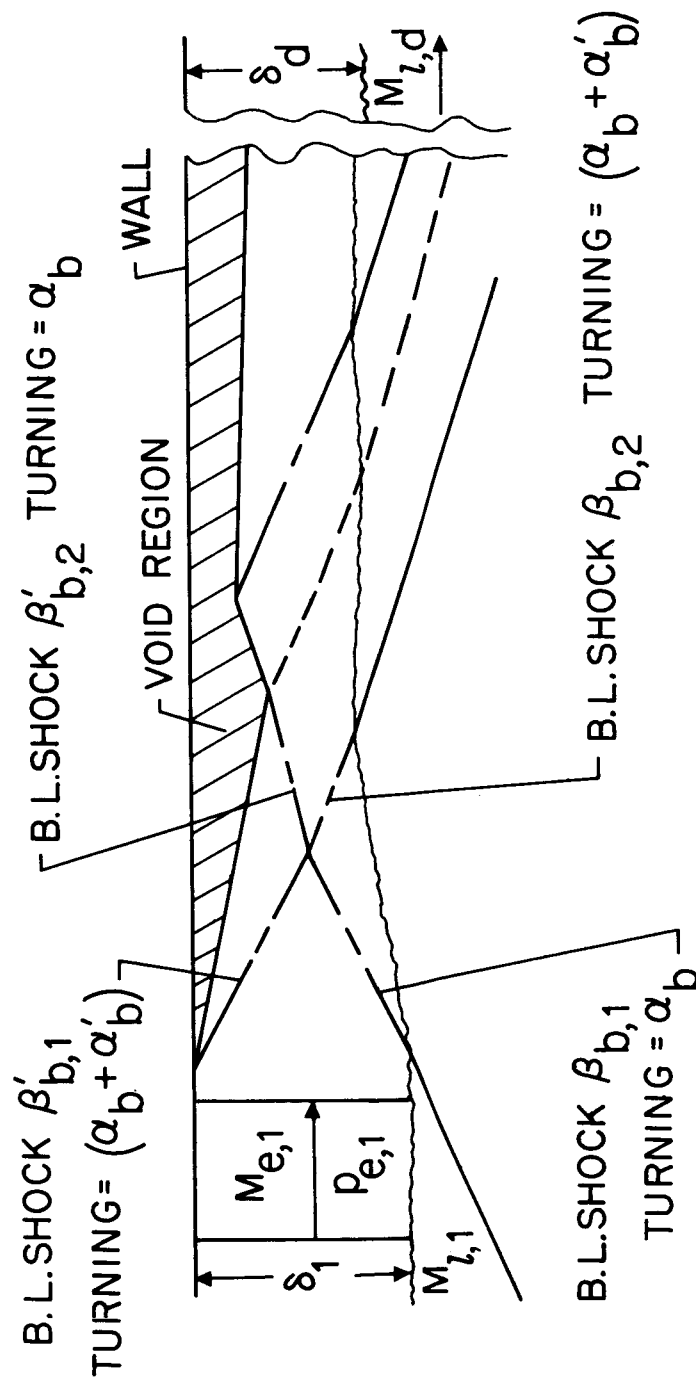
(a) Shock waves.

Figure 4.- Boundary-layer shock model for $(z_1 \delta_1) \leqq \delta_1$.
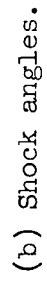
NASA

(b) Shock angles.

Figure 4.- Concluded.

NASA

(a) Shock waves.
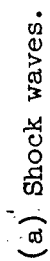
Figure 5.- Boundary-layer shock model for $(z_1 \delta_1) > \delta_1$.
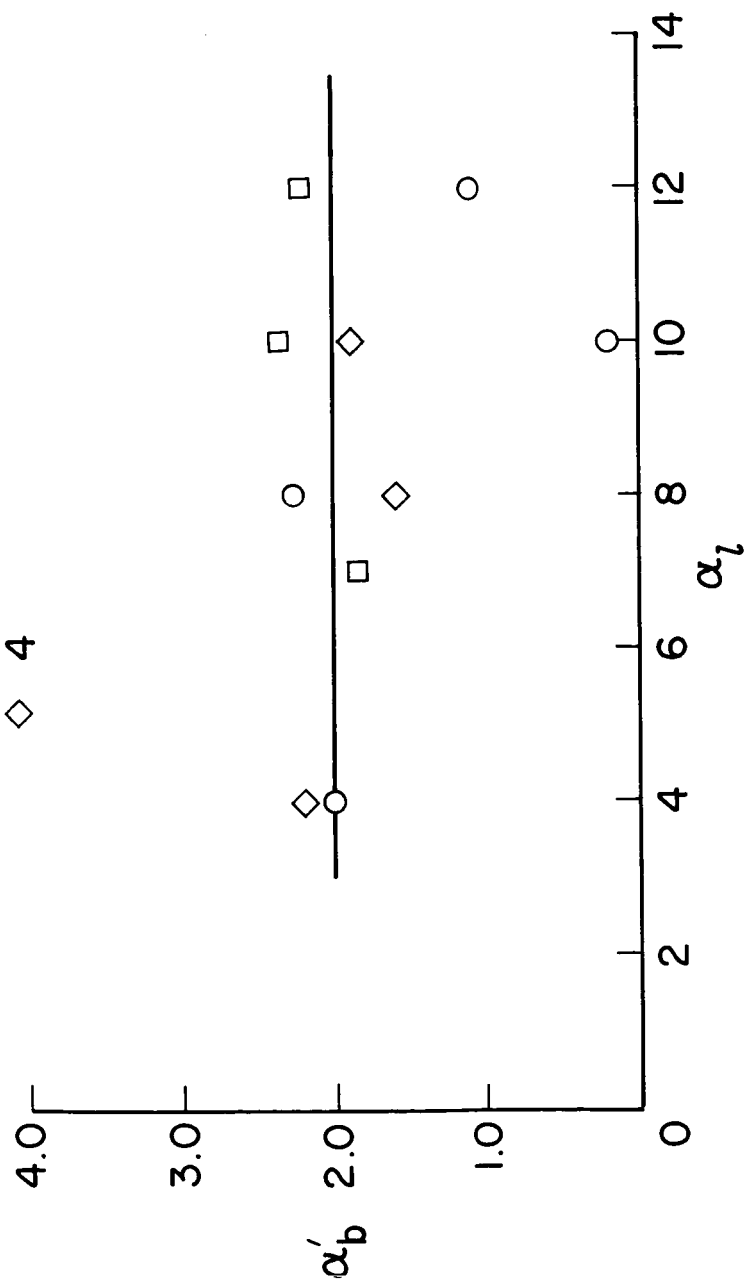
NASA

(b) Shock angles.

Figure 5.- Concluded.

Figure 6.- Values of α_b' calculated from data versus α_l.

NASA
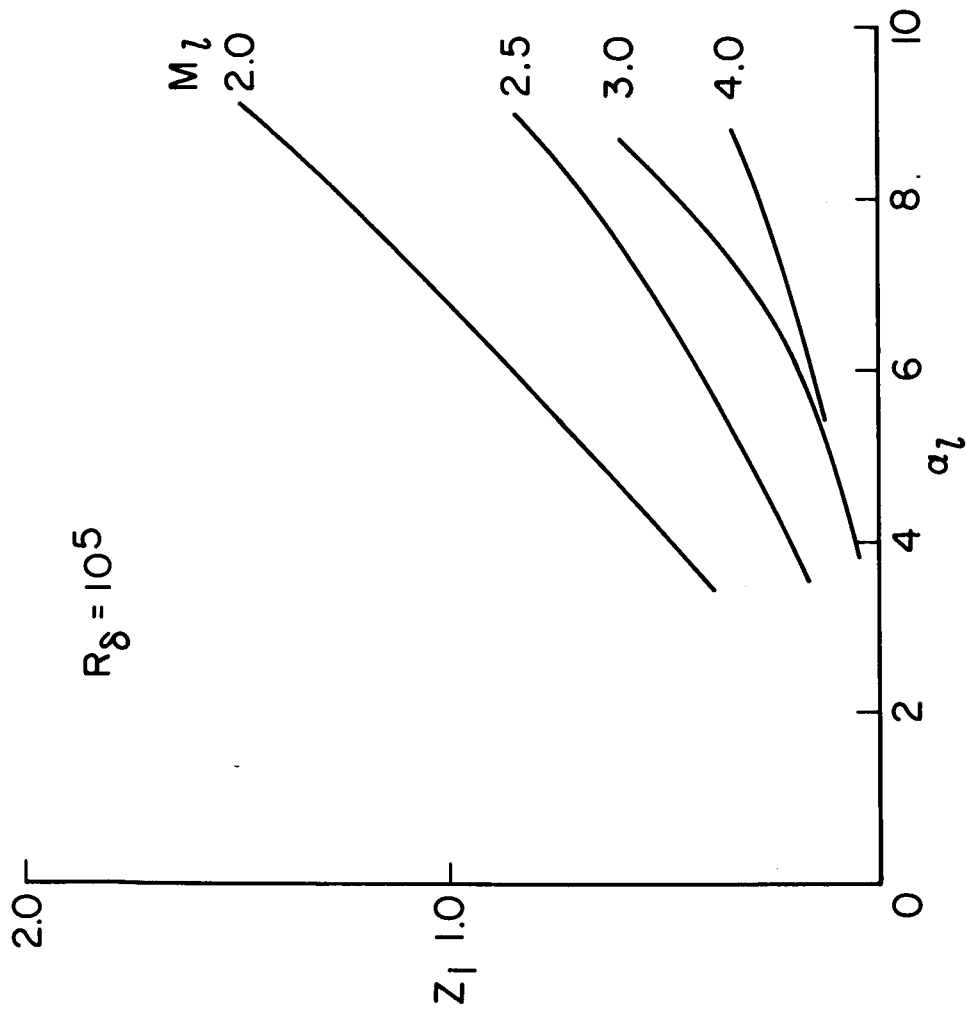
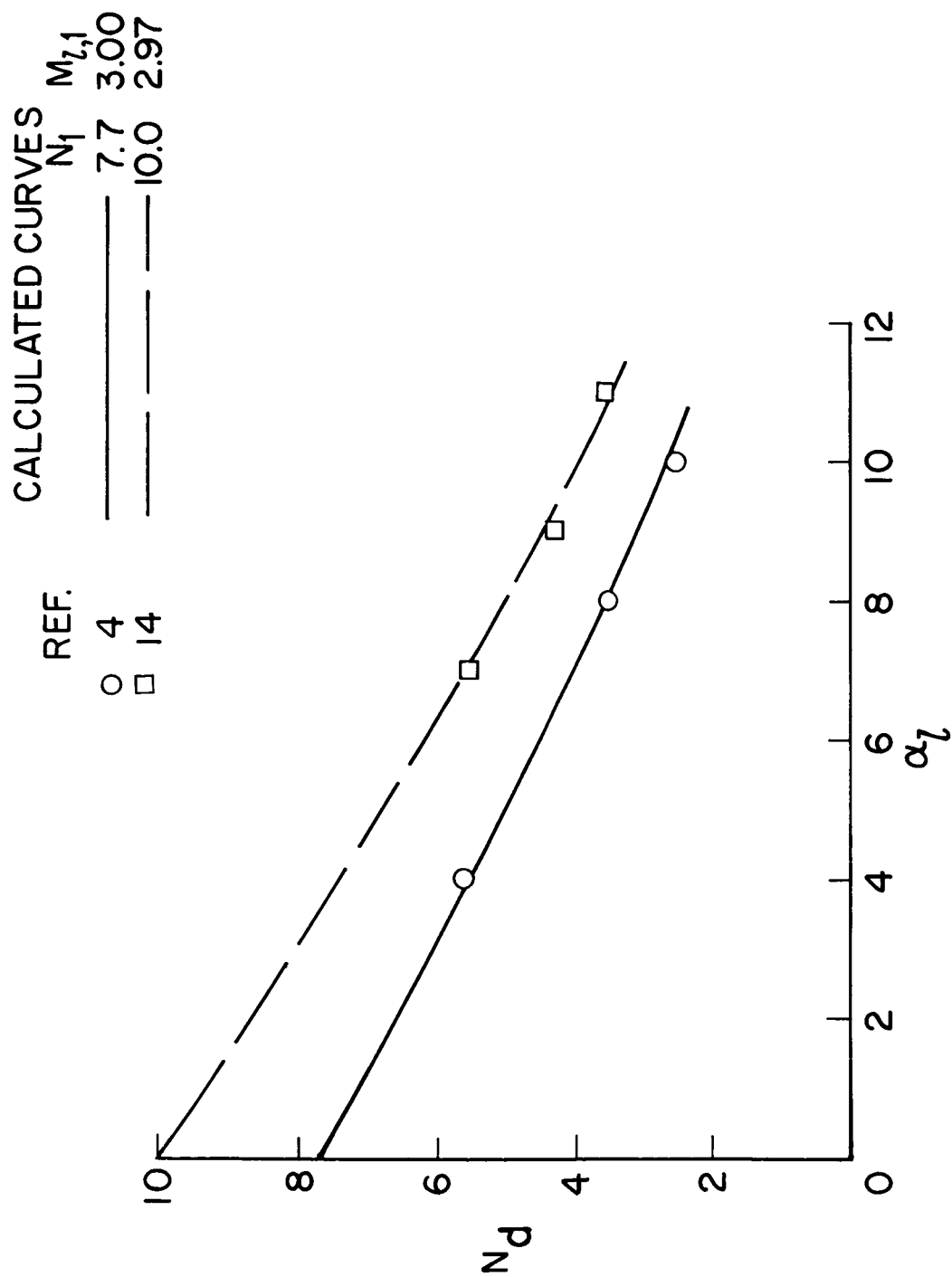Figure 7.- Effect of turning angle and Mach number on Z_1.

NASA

CALCULATED CURVES

N_l	$M_{l,1}$
7.7	3.00
10.0	2.97

REF.

○ 4
□ 14

N_d

α_l

0 2 4 6 8 10 12

2 4 6 8 10

NASA

Figure 8.- Calculated profile parameter N_d compared with data.

NASA

PRESENT
METHOD   REF.   DATA

———   7   ○
— — —   6   □
— · — ·   4   ◇

1.2

1.0

.8

.6

$\left(\dfrac{\delta_d}{\delta_1}\right)$

FROM DATA Z_2

FROM CALCULATED Z_2

1.0

.8

.6

0   2   4   6   8   10   12   14
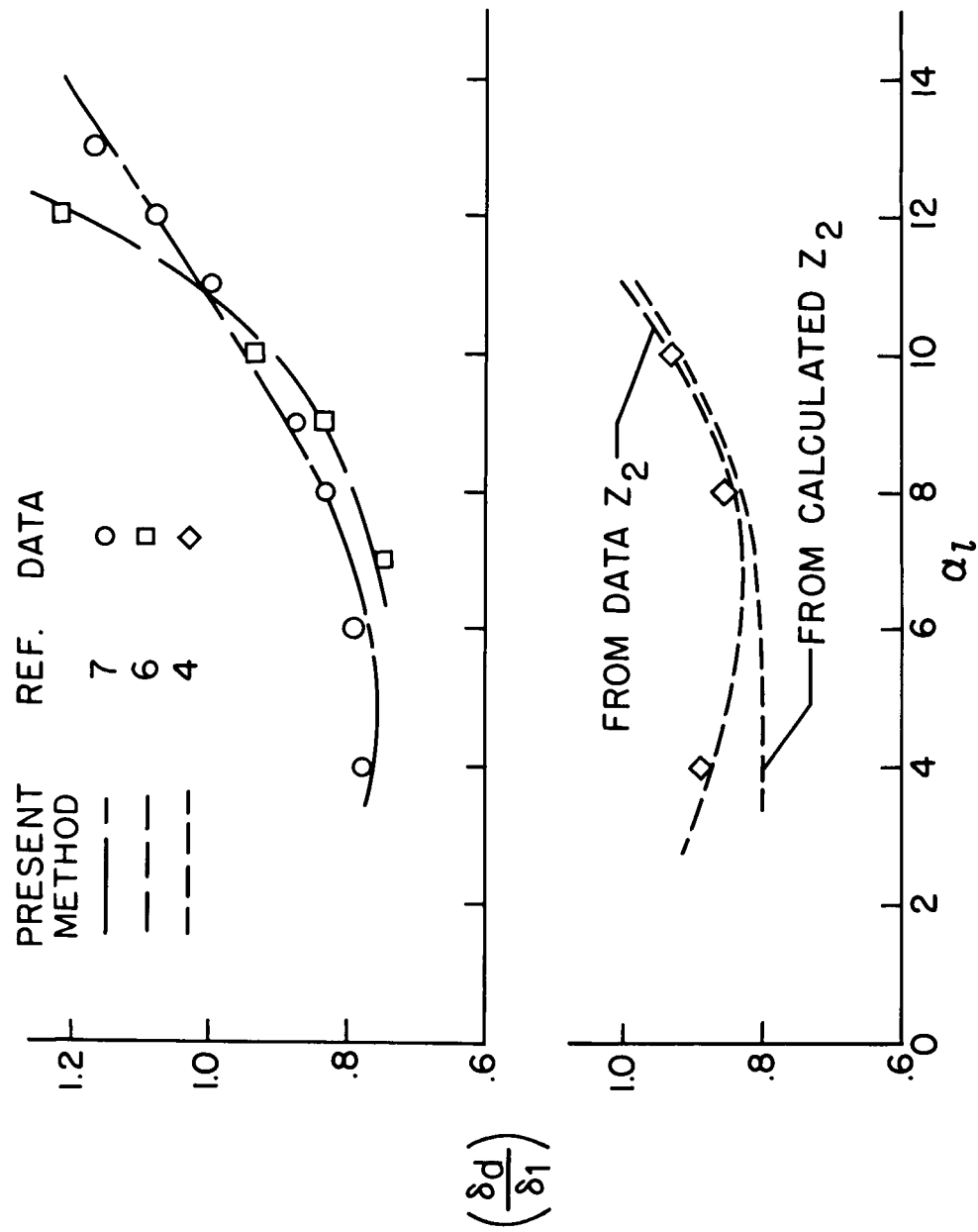
α_l

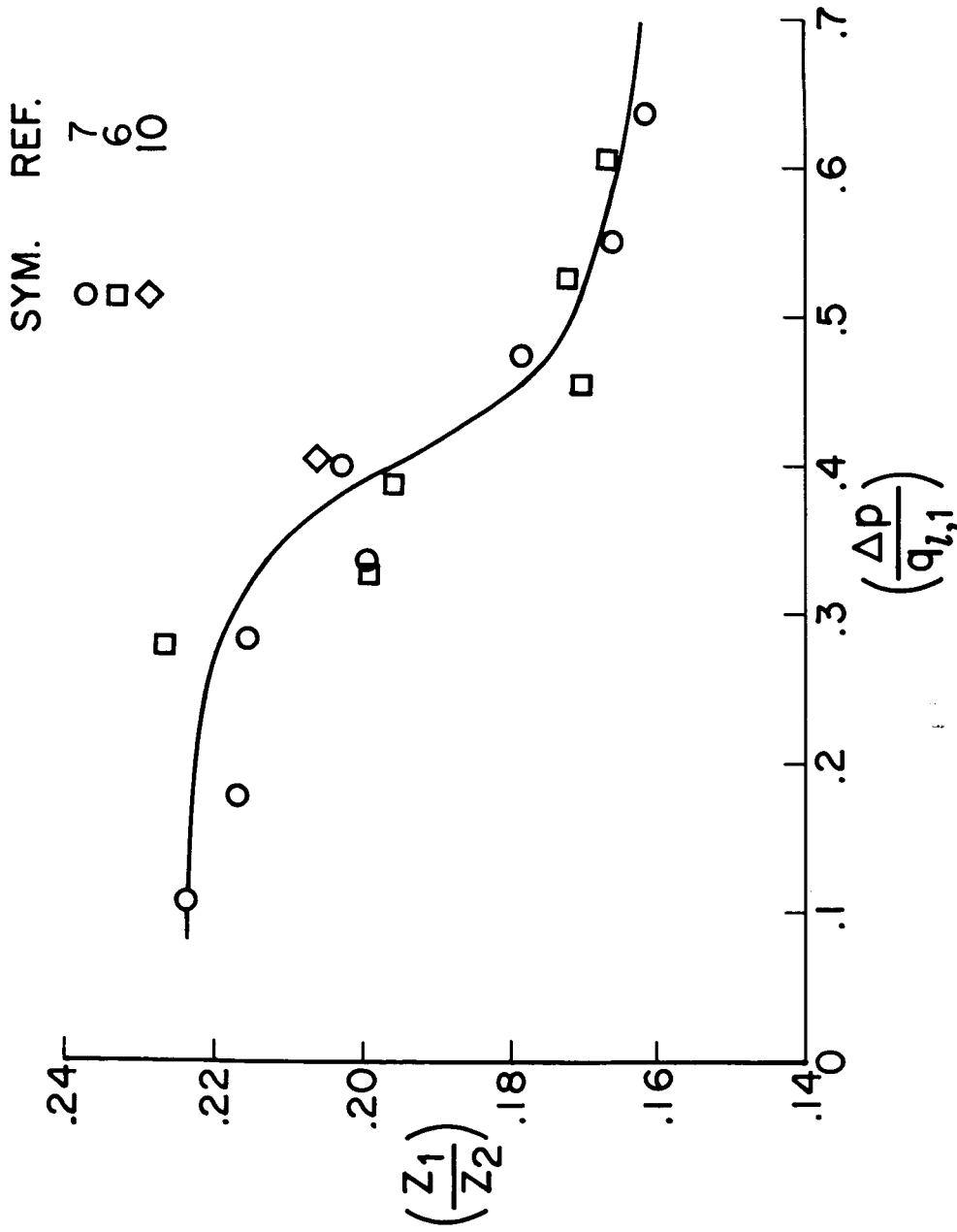Figure 9.- Calculated $\dfrac{\delta_d}{\delta_1}$ compared with data.

Figure 10.- Free stream $\left(\dfrac{\Delta p}{q_{l,1}}\right)$ across a shock versus $\left(\dfrac{z_1}{z_2}\right)$.
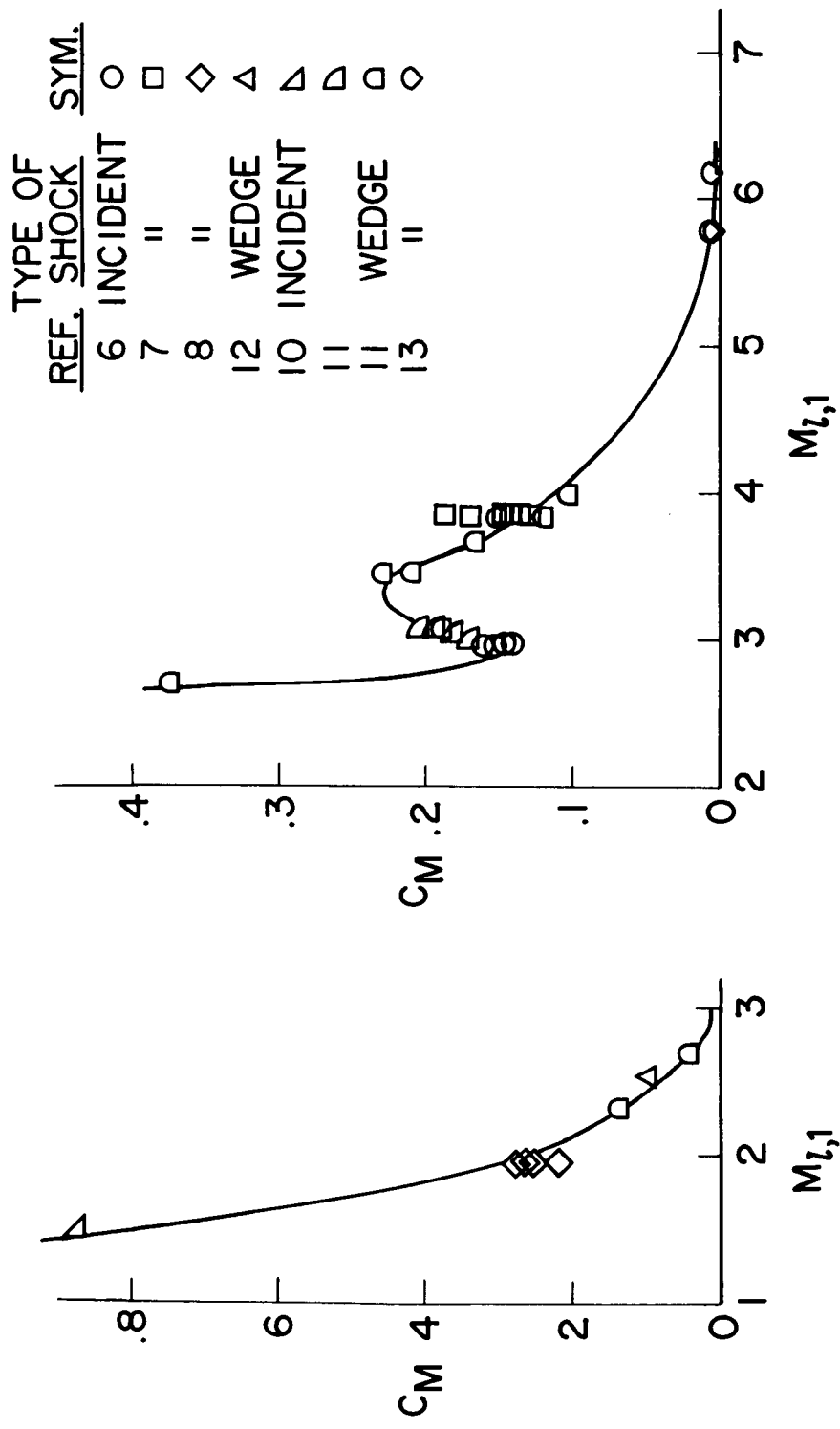
NASA

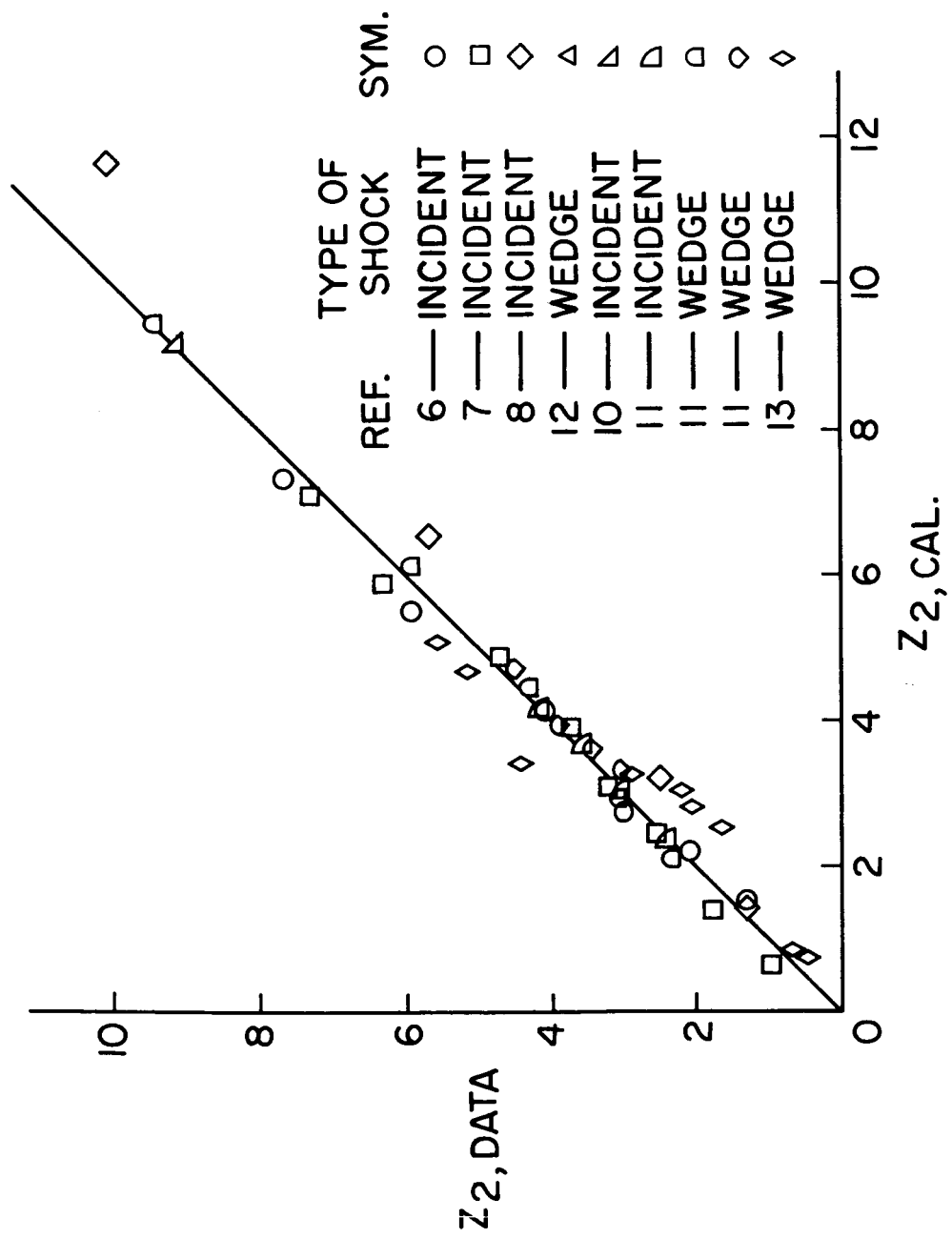Figure 11.- Mach number function C_M used in calculating z_2.

NASA

TYPE OF
SYM.

REF.	SHOCK	SYM.
6 ——	INCIDENT	○
7 ——	INCIDENT	□
8 ——	INCIDENT	◇
12 ——	WEDGE	◁
10 ——	INCIDENT	△
11 ——	INCIDENT	◺
11 ——	WEDGE	◻
11 ——	WEDGE	◇
13 ——	WEDGE	◇

Z_2, CAL.

Z_2, DATA

Figure 12.- Calculated Z_2 versus data Z_2.